ASSOCIATION BEHAVIORS OF COAL-DERIVED MATERIALS IN ORGANIC SOLVENTS

Masashi Iino
Institute for Chemical Reaction Science,
Tohoku University
Katahira, Aoba-ku, Sendai 980-8577, JAPAN

KEYWORDS: Coal-derived material, coal extract, association, organic solvent

INTRODUCTION

Coal-derived materials such as coal extracts and liquefaction products are known to readily associate in organic solvents(1,2). Hydrogen bonds and aromatic π–π interactions are considered to be main associative interactions, though charge transfer and ionic interactions possibly contribute to the associations. Many studies on this topic have been carried out so far, since these association behaviors strongly affect solubility, boiling point, viscosity, and other phisical properties at their bulk or solution state, which are key properties in the operation of coal conversion processes.

This topic is also related to controversial issue in coal structure i.e., covalent crosslinking network or non-covalent (molecular associated) network. Coal swells in an organic solvent and a swollen coal shows elastic behaviors. So, it is sure that coal has a kind of network structure. Although covalently connected crosslinking network structures are often assumed so far, there is no clear evidence for them. Recent works (3-5) suggest that at least for some bituminous coals, non-covalently connected network, i.e., associate structures of coal molecules are a better model than the covalent ones.

Here, association behaviors of coal-derive materials will be reviewed and discussed from solubility, molecular weight, viscosity, surface tension, small angle neutron scattering, and computor simulation, compared with petroleum asphaltenes in solution. Thermodynamics of the solution will also be discussed from sol-gel transition phenomena.

RESULTS AND DISCUSSION

Solubilities.

It is well known that the solubilities of coal-derived materials increase by silylation, i.e., OH $\rightarrow$ $OSiC(CH_3)_3$ or actylation of OH groups. This can be attributed to loss of intermolecular hydrogen bonds among coal molecules. Similarly, the pyridine extraction yields of a high-rank bituminous coal (89.6 carbon %) increases from 5% to 90 % by C-octylation at carbons such as benzylic methylene carbons, probably due to the disruption of the π–π stacking of aromatic rings by the introduction of the large octyl group. (6)

We found (7. 8) that a 1:1 carbon disulfide / *N*-methyl-2-pyrrolidinone (CS_2 / NMP) mixed solvent gave high extraction yields, more than 50 wt%, for several bituminous coals at room temperature. No significant bond cleavage has been observed to occur during the extraction. The extracts obtained, i.e., the mixed solvent soluble fractions, were further fractionated with acetone and pyridine into acetone soluble (AS) fraction, acetone insoluble / pyridine soluble (PS) fraction, and pyridine insoluble (PI) fraction which is a heavier fraction than preasphaltenes. We also have found that 30 – 50 % of PI became insoluble in the extraction mixed solvent, but the solubilities recovered by the re-addition of the separated extract fractions (AS and PS) or the addition of the compounds which have strong interaction with coal molecules, to PI (9, 10). Especially, tetracyanoethylene (TCNE) and tetracyanoquinodimethane (TCNQ) were found to be very effective. The studies on IR spectra of the extract fractions and reversibility of the effect of TCNE addition suggest that the solubility increase is caused by the breaking of noncovalent bonds in associated structures of coal molecules by TCNE, which interact and form new associates with coal molecules which are soluble in the mixed solvent.

Molecular Weight

Hombach(11,12) indicated that usual osmometric methods including VPO is not recommended for molecular weight determinations for complex coal-derived substances, since the van't Hoff equation used for osmotic pressure is not applicable for the substances with polydispersed molecular weights and inhomogeneous chemical structures such as coal asphaltenes. Collins et al.(13) also suggested that there is no accurate method for the molecular weight determinations of coal-derived substances, since coal solutions can not be viewed as a solution of a series of polymer homologues which is a necessary condition for use of osmotic or light-scattering methods. Hombach(12) has reported that a fraction obtained by ultrafiltration (0.2 and 0.035 μm pore filter) in pyridine solution of pyridine extract from a solubilized bituminous coal have very high molecular weights, i.e., 1.59×10^6 using a low-angle laser light-scattering method. Larsen et al.(14) showed that for relatively low molecular weight coal-derived substances mass spectrometry is available, and molecular weights determined by ^{252}Cf plasma desorption mass spectrometry are in good agreement with those obtained by field ionization mass spectrometry and gel permeation chromatography. Asphaltenes from distillation residues of liquefaction products of various coals have 260 - 330 of number-average molecular weight by ^{252}Cf plasma

desorption mass spectrometry.

Lee et al.(15) used VPO as a means for determination of degree of association of coal-derived substances. From the relation between molecular weight and concentration of coal-derived substances in solution, the dissociation constants of dimer, trimer, and higher multimers, and their distribution change with concentration were determined.

Viscosity

Viscosity of coal-derived substances in solution and bulk is related to their associated structures, and in coal liquefaction processes it is important to control high viscosity of coal – solvent mixtures. Bockrath et al.(16) measured the viscosities of preasphaltene, asphaltene (and its acid / neutral and basic components), and oil (pentane soluble) of coal-derived liquids from liquefaction. The viscosity of the mixtures of various compositions of acid / neutral and basic asphaltenes for fixed total asphaltene fraction (30 % asphaltene in oil) was found to be greater than would be expected on the basis of a simple additive relationship, suggesting that hydrogen bonding between acid / neutral with basic asphaltenes increases viscosity. The preasphaltenes, on a weight basis, have approximately twice the effect on viscosity as do the asphaltenes, probably due to their larger molecular weight and functionality in comparison to the asphaltenes. Bockrath et al.(17) also have showed that intermolecular association involving hydrogen bonding is a prime factor for the viscosity increase which occurred with increased asphaltene concentration in a reference solvent. Similarly the importance of hydrogen bonds largely involving phenolic OH in the viscosity increase was suggested.(18) Arganinski and Jones(19,20) also suggest that the influence on the viscosity of coal-derived preasphaltenes and model compounds in THF was the order hydrogen bonding > molecular weight >> degree of aromatic condensation (charge transfer interaction).

Surface Tention

Surface tension is used for analyzing colloidal properties such as micelles formation. We(21) measured the surface tension of *N*-methyl-2-pyrrolidinone (NMP) solution of acetone soluble (AS) and acetone insoluble / pyridine soluble (PS) fractions of the CS_2 / NMP mixed solvent extract of a bituminous coal by the Wilhelmy method. The surface tensions of the solutions freshly prepared by the dilution of the concentrated solution with NMP changed with time, and it took several hours to attain an equilibrium state of lower surface tension. This suggests that the rate of the re-construction to a new association state are very slow. The equilibrium surface tensions of NMP solution of AS decreases with AS concentration and a discontinuity point at some concentration (0.1 – 0.3 g/dL for two different As's) are observed, where the slope in the surface tension - ln c plots changes, suggesting that at this concentration association state abruptly changes, such as the formation of micelles. The discontinuities observed in this study are not so distinct as the case reported for pyridine solution of a petroleum asphaltene by Sheu et al..(22) The discontinuity concentration for the petroleum asphaltene was also found to be about 0.03 g/dL, one order lower than those for the coal extracts, reflecting the difference of micelle structures probably due the difference between chemical structure, molecular weight and shape of both constituents. For PS from the same coal as AS, on the other hand, discontinuity was not observed. Further study is needed to clarify this.

Small-Angle Neutron Scattering

Although small-angle neutron scattering (SANS) studies on the size distribution and shape of petroleum asphaltene associates in solution have been actively carried out, only a few SANS studies on coal-derived substances were reported so far. Cody, Thiyagarajan et al.(23,24) measured SANS of deuteropyridine solutions of pyridine extracts and their O-methylated derivatives. Laser desorption mass spectrometry of the extracts, untreated and methylated, indicates a predominance of relatively low mass materials, with molecular weight of the order 300 and a mass envelope which tails off around a thousand daltons.(23) SANS indicates that the solution structure of the extracts exists as small particles, with radii about 80 Å, and the values of fractal dimension, d (<3) indicates that the small particles further form a randomly assembled, loosely extended aggregates. Considering the molecular weights and radii for the particles, the elemental particles are themselves aggregates of the extract molecules. O-methylation is expected to decrease aggregation and/or make aggregates more loose, since hydrogen-bonding interactions are considered to constitute the dominant associative interparticle interaction. However, the change in the solution state due to O-methylation was found to be slight, and it induces more densed packing of aggregates for the two coals, in which d increases by O-methylation.

SANS data on the CS_2 / NMP mixed solvent extracts in solution by Cody, Thiyagarajan et al.(25) are interesting. The solution of pyridine insoluble / the mixed solvent soluble component, PI in the mixed solvent contains no large aggregates, but the solution of pyridine extract from the same coal, which may be a lighter component than PI, contains large aggregates, though a light component seems less aggregative due to low content of functional groups. Recently we found that addition of 2 wt% of TCNE relative to the amount of PI results in an enortmous change in the SANS behabior, namely, the addition of TCNE reduces the particle (associates) size greatly. This agrees with the enhanced extractability and solubility in CS_2/ NMP mentioned above by the addition of TCNE, considering that the size reduction of the associates of coal molecules makes

themselves more soluble in CS_2 / NMP. This result seems to give a direct evidence for the dissociation of the aggregates of coal molecules by TCNE through its strong interaction ability with coal molecules. However, our recent results (10) shows that some derivatives formed from TCNE may be responsible for the increase in solubility, rather than TCNE itself. So, the mechanism seems more complex than we considered so far. Further detailed study on the effect of TCNE and other additives such as PCP on SANS behaviors of coal extract solutions is needed to clarify the mrchanism for the enhanced extractability and solubility in CS_2/ NMP.

Sol-Gel Transition

To date, no experimental data on sol-gel transition lines are reported on coal related materials. We are trying to address this important gap by direct measurement of sol-gel transition lines of coal related material-solvent mixtures. Our attention is focused upon thermoreversible gelation of coal extracts in organic solvents.

Many earlier studies have approached this problem by investigating rubbery or gelly coal - solvent and extracted coal - solvent systems (26-28) . Based on studies of polymeric gels, it was generally believed that mostly relatively "poor" solvents were capable of gel formation. However, physical-thermoreversible gelation can take place in good solvents due to compound-compound and compound-solvent interactions. This kind of molecular aggregation has been widely observed in polymer-solvent systems, where gels are formed on cooling and disappear on heating. In contrast to the high molecular weight polymers, it has been discovered lately (29) that some lower molecular weight organic compounds (300 - 1000 daltons) can form thermoreversible gels with some organic solvents. Likewise, we have also observed that 2-naphthol (MW = 144 daltons) can form gels with N-methyl-2-pyrrolidinone (NMP). Intuitively speaking, the thermoreversible gelation could be a common feature in organic compound - solvent systems.

In this work we are interested particularly in the thermoreversible gelation in good solvents. Here, we introduce our preliminary approach to make direct measurements to determine the sol-gel transition lines for coal extracts and extract fractions using methods developed for polymer-solvent solutions. So far, no detailed thermodynamic analyses are attempted. In the present program of study we have been using various methods: a standard differential scanning calorimetry, a ball drop method and a thermogravimetric technique. a ball drop method was used to study "gel melting" lines. Experiments were carried out by cooling samples slowly to -30°C and then observing capabilities of solutions to keep 60 mg balls during heating with a rate about 0.5 °C/min. This type of experiment allows us to classify a substance presumably as a "gel" if its network is sufficiently stiff to withstand the 60 mg ball drop due to gravity. Preliminary experimental results using various extracts from Upper Freeport coal will be shown.

Computer Simulation

Computer-aided molecular design (CAMD) has been utilized in the designs of the drugs and new functional materials. Recently, it has been applied to coal.(30-33) Energetically stable three dimensional structure (conformation) of the extract fractions of coal was constructed by computer simulation.(33) The most stable structure in the energy-minimum state for model molecules PS, obtained from the CS_2/ NMP mixed solvent extraction of a bituminous coal was estimated to be an associated structure and the $\pi-\pi$ interactions between aromatic ring systems play a major role to form the association.

REFERENCES

1. Sternberg, H. W., Raymond, R. and Schweighardt, F. K., *Science*, **1975**, 188, 49.
2. Stenberg, V. I., Baltisberger, R.J.,and Patel, K. M. et al., *Coal Science* (ed Gorbarty, M. L.,Larsen, J. W., Wender, I.), Academic Press, *New York*, **1983**, 125-171.
3. Nishioka, M., *Fuel*, **1992**, 71, 941.
4. Cody, G. D., Davis, A.and Hatcher, D. G., *Energy Fuels*, **1993**, 7, 455.
5. Liu, H., Ishizuka, T., Takanohashi, T. and Iino, M., *Energy Fuels*, **1993**, 7, 1108.
6. Miyake, M. and Stock, L.M., *Energy Fuels*, **1988**, 2, 815.
7. Iino, M., Takanohashi T., Ohsuga, H. and Toda, K., *Fuel*, **1988**, 67, 1639.
8. Iino, M., Takanohashi, T., Obara, S., Tsueta, H. and Sanokawa, Y., *Fuel*, **1989**, 68(12), 1588-1593.
9. Sanokawa, Y., Takanohashi, T. and Iino, M., *Fuel*, **1990**, 69, 1577.
10. Iino, M., Kurose, H. Giray, E. S., and Takanohashi, T., *Prepr. Pap. Am. Chem.Soc.,Div. Fuel Chem.* **1998**, 43(3),712-716.
11. Hombach, H.-P., *Fuel*, **1981**, 60, 663.
12. Hombach, H.-P., *Fuel*, **1982**, 61, 215.
13. Collins, C.J., Triolo, R. and Lietzke, M.H., *Fuel*, **1984**, 63, 1202.
14. Larsen, J.W., Lapucha, A.R., Wernett, P.C. and Anderson, W.A., *Energy Fuels*, **1994**, 8, 258.

15. Lee, W.C., Schwager, I. and Yen, T.F., *Prepr. Pap.-Am. Chem. Soc., Div. Fuel Chem.*, **1978**, 23(2), 37.
16. Bockrath, B.C., Lacount, R.B. and Noceti, R.P., *Fuel Process.Technol.*, **1978**, 1, 217.
17. Bockrath, B.C., Lacount, R.B. and Noceti, R.P., *Fuel*, **1980**, 59, 621.
18. Taylor, S.R. and Li, N.C., *Fuel*, **1978**, 57, 117.
19. Jones, M.B. and Argasinski, J.K., *Prepr. Pap.-Am. Chem. Soc., Div. Fuel Chem.*, **1985**, 30(4), 250.
20. Argasinski, J.K. and Jones, M.B., *Prepr. Pap.-Am. Chem. Soc., Div. Fuel Chem.*, **1987**, 32(1), 604.
21. Hayasaka, K., Takanohashi, T. and Iino, M., *Energy Fuels*, **1996**, 10, 262.
22. Sheu, E.Y. and Storm, D.A., *Fuel*, **1994**, 73, 1368
23. Cody, G.D., Thiyagarajan, P., Botto, R.E., Hunt, J.E. and Winans, R.E., *Energy Fuels*, **1994**, 8, 1370
24. Thiyagarajan, P., Cody, G.D., Hunt, J.E. and Winans, R.E., *Prepr. Pap.-Am.Chem. Soc., Div. Fuel Chem.*, **1995**,40(3),397.
25. Cody, G.D., Obeng, M. and Thiyagarajan, P., *Energy Fuels*, **1997**, 11, 495.
26. Hall, P. J., and Larsen, J. W., *Energy Fuels* **1991**, 5, 228.
27. Gody, G. D., and Painter, P. C., *Energy Fuels* **1997**, 11, 1044.
28. Takanohashi, T., Kudo, T., and Iino, M., *Energy Fuels* **1998**, 12, 470.
29. Yasuda, Y., Iishi, E., Inada, H., and Shirota, Y., *Chemistry Letters* **1996**, 575.
30. Carlson, G.A., *Energy Fuels*, **1992**, 6, 771.
31. Faulon, J.L., Hatcher, K.A. P.G., Carlson, G.A. and Wenzel,K.A., *Fuel Process. Technol.*, 34, 277 (1993)
32. Nomura, M., Matsubayashi, K., Ida, T. and Murata, S., *Fuel Process. Technol.*, **1992**, 31, 169
33. Takanohashi, T., Iino, M.. and Nakamura, K. *Energy Fuels*, **1994**, 8, 395

PROBING COAL REACTIVITY BY TIME-RESOLVED SMALL ANGLE X-RAY SCATTERING

R. E. Winans, S. Seifert, and P. Thiyagarajan†
Chemistry Division and †Intense Pulsed Neutron Source Division
Argonne National Laboratory
Argonne, IL 60439

Keywords: Argonne coal swelling, time-resolved small angle neutron scattering

ABSTRACT

The objective of this study is to observe changes in coal structure in situ with small angle X-ray scattering (SAXS) during solvent swelling and during pyrolysis. We have built a SAXS instrument at the Basic Energy Sciences Synchrotron Research Center at the Advanced Photon Source that allows us to obtain scattering patterns in the millisecond time domain. The eight Argonne Premium Coal samples were used in this study. The information that can be derived from these experiments, such as changes in fractal dimensionality and in size and type of porosity, was found to be very rank-dependent. In the swelling experiments, it was noted that for certain coals, structural changes occurred in just a few minutes.

INTRODUCTION

Coal solvent interactions have been studied extensively over the last 25 years. Most coals swell significantly in solvents such as pyridine and this effect has been exploited to study the macromolecular structure of coals (1-8). Typically, the volumetric swell ratio (Q_v) is measured and is defined as the ratio of the swollen volume over the dry volume. Recently, the swelling of individual particles was determined using microscopy combined with video and image analysis (9). Otake and Suuberg studied the temperature dependence of the rate of swelling on some of the Argonne Premium Coal Samples (10). Also, they looked at a larger set of low rank coals (11). They found large differences in the rate of coal swelling with the Illinois No. 6 (APCS 3) being the fastest and the lignite (APCS 8) the slowest. The Upper Freeport (APCS 1) has been studied extensively in part due to its unusually large solubility in the NMP/CS_2 mixed solvent system (12).

Small angle neutron scattering (SANS) has been used to study swollen coals and extracts. For the Pittsburgh coal (APCS 4), it was shown that a rod-like pore structure developed upon swelling in pyridine (13). It has also been shown that pyridine solubles are not truly soluble (14). Finally, the Upper Freeport coal was studied extensively with SANS on both soluble and insoluble fractions for NMP/CS_2 and pyridine (15).

The present study exploits the brilliance of the undulator X-ray source at the Advanced Photon Source to probe, in real time, the structure changes in coal swelling using SAXS. The information derived from the SAXS experiment throws new light on the early stages of structure changes in coal swelling.

EXPERIMENTAL

The eight Argonne Premium Coal Samples were used without modification in this study (16). The SAXS instrument was constructed at ANL and used on the Basic Energy Sciences Synchrotron Radiation Center CAT undulator beamline ID-12 at the Advanced Photon Source (http://www.bessrc.aps.anl/).

Quartz capillaries (1 mm) were used to sample 5 mg of -100 mesh coal. Scattering patterns were obtained on the dry coal, then 10 μl of solvent was added with a syringe such that all the sample was wetted. SAXS data were obtained every minute for one hour with approximately a one minute delay after adding the solvent. Monochromatic X-rays (8.5 - 23.0 keV) are scattered off the sample and collected on a 19 x 19 cm^2 position sensitive two-dimensional gas detector. The scattered intensity has been corrected for absorption, the empty capillary scattering, and instrument background. The differential scattering cross section has been expressed as a function of the scattering vector Q, which is defined as:

$$Q = \frac{4\pi}{\lambda} \sin \theta$$

where λ is the wavelength of the X-rays and θ is the scattering half angle. The value of Q is proportional to the inverse of the length scale ($Å^{-1}$). The instrument was operated with two different sample-to-detector distances, 68.5 cm to obtain data at $0.04 < Q < 0.7$ $Å^{-1}$ and 3740 cm to measure at $0.006 < Q < 0.1$ $Å^{-1}$.

Small Angle X-ray Scattering

A typical two-dimensional plot of the time-resolved data for the swelling of the subbituminous coal (APCS 2) in pyridine is shown in Figure 1. These curves can be analyzed to determine size of features, topology, and changes in total scattering. At small Q in the Guinier region, the radius of gyration (R_g), which is related to the size of the scattering features, can be determined. For example, R_g for spheres can be determined from the slope of I(Q) vs Q^2 in a Q region where $R_g Q \leq 1.0$. Power law slope (fractal dimension) from the data, such as is shown in Figure 1, are used to describe the topology of the system. Finally, the invariant Q_0 is calculated and is proportional to the fluctuation of the electron density in the system. Changes in the invariant are useful in monitoring topological changes in the sample.

$$Q_0 = \int_0^\infty I(Q)\, Q^2\, dQ$$

For example, the invariant goes to zero for a homogeneous system such as a solution of coal molecules that are truly soluble and not aggregated.

RESULTS AND DISCUSSION

This discussion will focus on four of the Argonne coals: lignite, Illinois #6, subbituminous, and Upper Freeport. The slowest swelling coal, lignite (APCS 8), at 25 °C took 230 min. to reach 50% of final swelling (t_{50}) (10), while the Illinois #6 at 24 °C had a t_{50} of 1.7 min. The subbituminous coal was chosen since its swelling rate is of an intermediate value, t_{50}=12.8 min. at 24 °C and its results correlate well with those described in the literature (10). Finally, the Upper Freeport was examined with two solvent systems, pyridine and NMP/CS_2 with very different results between the two solvents.

A set of sixty scattering curves are shown in Figure 1 for the subbituminous coal in pyridine. Initially, there are only small changes, then between 10 and 25 min., the slope and invariant decreased quite rapidly. The change in fractal dimensions is shown in Figure 2 for all four of the coals. It appears that the decrease in the fractal dimension is stopped when the subbituminous coal is fully swollen. Between 10 and 35 min. this data fits an exponential decay with a constant of 0.16 $min.^{-1}$. For short length scales < 30Å, there appears to be an increase in the scattering when the swelling has finished. After the macromolecular structure has expanded, changes at the molecular level can be discerned.

The swelling of Illinois #6 was very rapid, therefore, the changes seen with time in the SAXS data must be due to a molecular aggregation that started after 20 min. However, this new configuration was not stable and slowly rearranged between 30 and 60 min. This was seen much better in the changes of the power law slope as shown in Figure 2. This unusual phenomenon was reproducible and appeared limited to the Illinois coal.

At room temperature, no changes in either the invariant or power law slope were observed for the lignite coal. However, the experiment was repeated at 50 °C, where $T_{50} \approx 25$ min. At low Q, the power law slope decreased, but this change was much smaller than those observed for the other coals. These higher temperature experiments need to be run at high Q to see if changes on a smaller length scale is occurring. In addition, acid treated lignite will be studied. There is considerable organic acid-mineral interactions in lignite.

The Upper Freeport mv bituminous coal does not swell as well as other coals, $Q_v = 1.3$ (12), while all the other lower rank coals swell with $Q_v \geq 2.0$. In NMP/CS_2, the ratio was not measured on the raw coal since it is very soluble (12). In pyridine, a rapid increase in the invariant occurred and then it remained constant after approximately 10 min. (see Figure 3). While the invariant in NMP/CS_2 starts at about the same value and does increase, the magnitude of the increase is much less, and after 10 min., it starts to decrease. Pyridine must decrease the surface area in the coal possibly by dissolution followed by re-aggregation. We know from SANS that pyridine solutions are actually aggregates (14). It is interesting that while NMP/CS_2 is a good extraction solvent for the Upper Freeport, it does not appear to greatly change the 3D structure on the length scales studied here.

CONCLUSIONS

Structure changes in initial solvent swelling are observed in the time-resolved SAXS data from the coals. With high rank coals in pyridine, there is a rapid breakup of the solid structure, followed by a re-aggregation that produces constant scattering. With NMP/CS_2, the effect is much smaller and the scattering decreases with time. For the subbituminous coal, the scattering increases immediately, probably forming a new pore structure with rod-like features.

ACKNOWLEDGMENTS

This work was performed under the auspices of the Office of Basic Energy Sciences, Division of Chemical Sciences and Division of Materials Sciences, U.S. Department of Energy, under contract number W-31-109-ENG-38. The support of the BESSRC staff is appreciated, especially Jennifer Linton and Mark Beno.

REFERENCES

1. Larsen, J. W.; Shawver, S. *Energy Fuels* **1990**, *4*, 74.
2. Cody, G. D.; Eser, S.; Hatcher, P.; Davis, A.; Sobkowiak, M.; Shenoy, S.; Painter, P.C. *Energy Fuels* **1992**, *6*, 716.
3. Hall, P. J.; Larsen, J. W. *Energy Fuels* **1993**, *7*, 47.
4. Suuberg, E. M.; Otake, Y.; Yun, Y.; Deevi, S. C. *Energy Fuels* **1993**, *7*, 384.
5. Yang, X.; Larsen, J. W.; Silbernagel, B. G. *Energy Fuels* **1993**, *7*, 439.
6. Ndaji, F. E.; Thomas, K. M. *Fuel* **1993**, *72*, 1525.
7. Aida, T.; Nawa, Y.; Shiotani, Y.; Yoshihara, M.; Yonezawa, T. *Conf. Proc. - Int. Conf. Coal Sci., 7th* **1993**, *2*, 445.
8. Larsen, J. W.; Gurevich, I.; Glass, A. S.; Stevenson, D. S. *Energy Fuels* **1996**, *10*, 1269.
9. Gao, H.; Artok, L.; Kidena, K.; Murata, S.; Miura, M.; Nomura, M. *Energy Fuels* **1998**, *12*, 881.
10. Otake, Y.; Suuberg, E. M. *Energy Fuels* **1997**, *11*, 1155.
11. Otake, Y.; Suuberg, E. M. *Fuel* **1998**, *77*, 901.
12. Takanohashi, T.; Iino, M.; Nishioka, M. *Energy Fuels* **1995**, *9*, 788.
13. Winans, R. E.; Thiyagarajan, P. *Energy Fuels* **1988**, *2*, 356.
14. Cody, G. D.; Thiyagarajan, P.; Botto, R. E.; Hunt, J. E., Winans, R. E. *Energy Fuels* **1994**, *8*, 1370.
15. Cody, G. D.; Obeng, M.; Thiyagarajan, P. *Energy Fuels* **1997**, *11*, 495.
16. Vorres, K. S. *Energy Fuels* **1990**, *4*, 420.

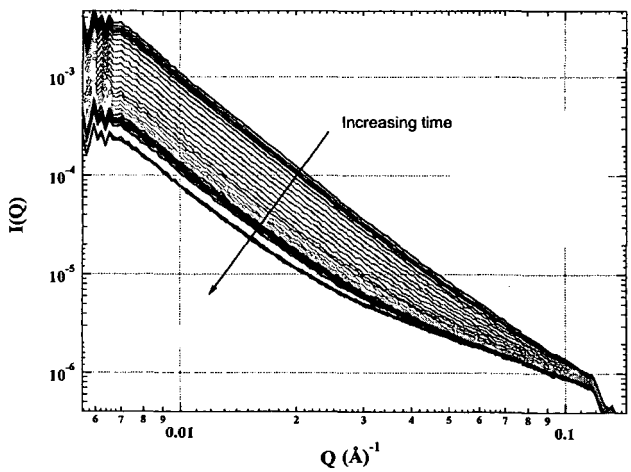

Figure 1. SAXS of the subbituminous coal (APCS 2) in pyridine from 1 to 60 minutes.

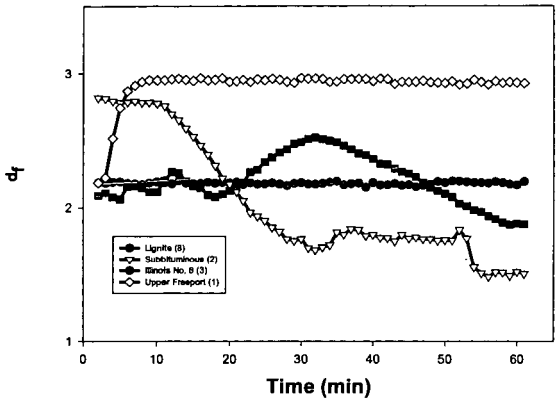

Figure 2. Power law slopes (fractal dimensions) for coal swelling in pyridine at low Q, as a function of solvent contact time.

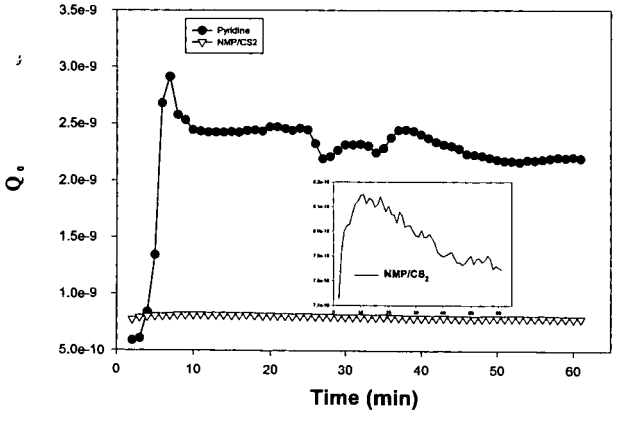

Figure 3. Invariant change with swelling in pyridine and NMP/CS_2 for the Upper Freeport coal. The inset is an exploded view in Q_0 for the NMP/CS_2 data.

MODELING PYROLYSIS BEHAVIOR FOR INTERNATIONAL COALS

M.A. Serio, M.A. Wójtowicz, S. Charpenay, Y. Chen, D.G. Hamblen, P.R. Solomon
Advanced Fuel Research, Inc.
87 Church Street, East Hartford, CT 06108-3742

Keywords: Coal Pyrolysis, Modeling, Coal Type

INTRODUCTION

Pyrolysis (devolatilization) is the initial step in most coal conversion processes, accounting for up to 60% of the initial weight loss from the coal. It is also the process that is most dependent on the organic properties of the coal, and is important because of its influence on the subsequent conversion process. The modeling of coal pyrolysis has progressed from simple, single equation kinetic models for overall weight loss to fairly complex "network" models. These models approximate coal as a polymeric structure and provide more detailed predictions of pyrolysis behavior than is possible with the simpler models. Professor Eric Suuberg has been involved for many years in the study of coal devolatilization modeling, pyrolysis kinetics, tar formation and vaporization, crosslinking reactions, network structure, thermochemistry of pyrolysis reactions, and char gasification and combustion reactivity [1-14]. All of the network model development efforts have greatly benefited from this body of work.

A total of three network coal devolatilization models have been developed, [15-19], which have various capabilities for predicting coal thermal decomposition under practical conditions. These coal devolatilization models are: (1) the Functional Group – Depolymerization, Vaporization, Crosslinking (FG-DVC) model [15-17], (2) the Chemical Percolation Devolatilization (CPD) model [18]; and the FLASHCHAIN model [19]. A common feature of the original versions of these models is that they required a large set of data inputs, including kinetic parameters, coal composition files, and additional parameters describing the coal polymeric structure. These input data could be generated on the basis of experimental measurements for each coal of interest, although this limited predictions to coals that had been studied. Alternatively, some investigators have tried to correlate the devolatilization properties to the coal types using simpler models. For instance, Ko *et al.* [20] and Neavel *et al.* [21] have developed methods for predicting the upper bound of tar yields, X_{tar}, from coal elemental compositions. Recently, successful efforts were made to retain the predictive capabilities of the network models, but with the ability to use ultimate analysis or comparable data to generate the input files. Niksa has developed a correlation method for the FLASHCHAIN model which predicts volatile yields in pyrolysis from ultimate analysis data [22-24]. A similar approach was used by Zhao *et al.* [25] to correlate the input parameter files for the FG-DVC model, while Fletcher and coworkers have used NMR data to correlate input parameters for their CPD model [26].

This paper briefly describes the historical development of one of the network models, the FG-DVC model [15-17], and how its development was influenced by the work of Professor Eric Suuberg. FG-DVC is a network coal devolatilization model which can predict, in addition to the tar and total volatile yields, the yields of individual gas species, the tar molecular weight distribution, and the char fluidity. It has also been coupled with a char reactivity model which incorporates the effect of thermally induced annealing on char reactivity. This model was primarily validated using data for North American coals and is now being extended to a range of international coals. This paper also discusses the progress of these efforts, along with the status and future prospects for coal devolatilization modeling activities in various parts of the world.

BACKGROUND ON FG-DVC MODEL

Coal has a very complicated organic structure, which is essentially a mixture of an aromatic matrix, side chain components, and some loose fragments. The thermal decomposition of the coal structure involves many parallel and competitive processes. In modeling these processes, FG-DVC uses two submodels. The FG model simulates the thermal evolution of various functional groups and the DVC model predicts the depolymerization, vaporization and crosslinking processes occurring in the coal polymer network. In the FG submodel, the gas evolution from functional group precursors is modeled with parallel first order reactions and a distributed activation energy (DAE) formulation is used to reflect the diversity of coal structures. In his doctoral thesis work at Massachusetts Institute of Technology [1,2,9] and in his academic work at the Carnegie-Mellon University [3,4,7], Prof. Suuberg and his colleagues pioneered the development of pyrolysis models which track individual species from coal using DAE kinetic models. These methods were adapted by researchers at Advanced Fuel Research, Inc. (AFR) for coal and related materials in the development of the FG-DVC model. More recently, Professor

Suuberg collaborated with AFR on a major review of pyrolysis experiments, kinetic rates and mechanisms, which summarized the progress in these areas and attempted to resolve the remaining controversies in the choices of kinetic rates and models [14].

The thermal evolution of the coal polymer matrix is modeled with a network model [16], which consists of nodes and the connections between them. The nodes represent the polymer clusters and there are two types of connections between them, i.e., weak and strong bonds and initial crosslinks. At elevated temperatures, there is a competition between bond breaking and crosslinking reactions, and the properties of the network are fully determined by these two competing processes through percolation theory calculations [27]. In the case of coal, cross-linking in the DVC subroutine is computed by assuming that this event is correlated with CO_2 and CH_4 evolutions predicted in the FG subroutine. The yield of rapidly released CO_2 (which is related to coal rank and weathering) is the factor that controls the thermosetting or thermoplastic behavior of coals, an observation that was first made by Suuberg and coworkers [5]. For coals which exhibit thermoplastic behavior, the fluidity is assumed to be limited by the cross-linking associated with the evolution of methyl groups [15-17].

The most important property of the network is the molecular weight distribution of the clusters. The heavy molecules remain in the condensed phase to become char, while the light ones evaporate to become tar. The model originally used the tar vapor pressure law of Unger and Suuberg [7], which was later modified by Suuberg *et al.* [4], and more recently improved by Fletcher *et al.* [26]. The tar rate is further limited by internal transport, which is assumed to be controlled by the evolution rate of gas species and the light tar [15]. This mechanism enables the model to predict the pressure variation of the tar yields.

A char reactivity model was developed as a submodel of FG-DVC [28]. The reactivity model can predict intrinsic reactivity based on correlations with char hydrogen content, coal oxygen content, and coal mineral content. A random pore model and a volumetric model are used for high rank and low rank coals, respectively, in order to predict variations of intrinsic reactivity with burnoff. In the pore diffusion regime, the model uses the Thiele modulus to calculate the reaction rate as a function of the intrinsic rate and char structural properties. The model includes the effects of thermal annealing on reducing the intrinsic char reactivity and also benefits from the work of Suuberg in this area [13].

The FG-DVC model was validated for the eight Argonne Premium coals [29] using measurements of pyrolysis kinetics from TG-FTIR analysis, solvent extraction and solvent swelling to measure extractables and the initial crosslink density, Gieseler plastometer experiments to measure fluidity, pyrolysis-FIMS to measure the tar molecular weight distribution, and ultimate analysis to determine the elemental compositions (C, H, N, S, O) [17]. The large number of experimental inputs allowed the development of a model which can make detailed predictions of coal devolatilization under various conditions of temperature, pressure, and heating rate.

A correlation method was subsequently developed which allows the FG-DVC model to be used for untested coals by providing an interpolation between the input files of known coals based on the coal elemental analysis [25]. The interpolation mesh is composed of nine coals: six from the Argonne Premium Coal Sample Program, and three from the Penn State Sample Bank (PSOC 1474, PSOC 1448, and PSOC 1521). Extensive experimental studies were carried out on these reference coals and the model input parameters are well established. With this scheme, any of the FG-DVC input parameters can be interpolated for an untested coal when its elemental composition is known.

RECENT DEVELOPMENTS IN MODELING OF COAL DEVOLATILIZATION

There are several recent developments and remaining challenges in the area of modeling coal devolatilization. Because of the globalization of coal markets, there is growing interest in predicting the pyrolysis behavior for a wide variety of coals from all over the world. Recent work at AFR has extended the range of FG-DVC model application to include South American, Japanese, Australian, South African, Indonesian, European, and Chinese coals [30]. Niksa has developed his FLASHCHAIN model to be applicable for a wide range of coal types [22-24]. This model has been recently incorporated into the EPRI NO_x-LOI predictor. In this expert system, the FLASHCHAIN model provides the underlying basis for predicting NO_x formation and unburned carbon formation (LOI) in a power plant by calibration against a known coal [31]. Since the partitioning of nitrogen species in pyrolysis has an important influence on NO_x formation in combustion, this aspect of devolatilization modeling has recently received increased attention [31-33].

For the same reasons, there has been increased interest in the incorporation of network devolatilization models into Comprehensive Fluid Dynamic (CFD) codes. Until recently, all of the commercial CFD codes incorporated relatively simple coal devolatilization models. The FG-DVC model has been integrated with research CFD codes, such as the Brigham Young University (BYU) PCGC-2 code and the DOE MFIX fluidized bed code [34,35]. The CPD model was recently integrated with the commercial FLUENT code [36], and the preliminary integration of FG-DVC with a CFD code has been accomplished at the University of Leeds [37]. AFR has also developed a streamlined version of the FG-DVC model which facilitates the integration process [38]. This version involves running the complete model outside the main CFD code and using it to define a set of coefficients that relate individual product evolution to a reference process (e.g., weight loss) over a prescribed range of conditions. AFR is also exploring artificial neural network (ANN) models for coal devolatilization which may result in another streamlined model [39]. In addition, a larger particle devolatilization version of FG-DVC has been developed for use as a submodel in fixed and fluidized bed systems [40].

Matthews *et al.* [41] have devised a molecular modeling approach to coal devolatilization which appears to be successful in predicting the general features of the mass loss and chemical structural changes for vitrinite samples heated in a drop tube. Work on molecular modeling of coal is also underway in Japan [42,43], although so far it has only been used to predict drying and coal/solvent interactions. Finally, coal devolatilization models are being adapted to predict related phenomena, such as coal liquefaction [44] and coal maturation [45].

CONCLUSIONS

During the past decade, the modeling of coal devolatilization has progressed from simple 1 or 2 step models to relatively complex network models. These models approximate coal as a polymeric structure and have demonstrated good predictive capability for a wide range of coal types and experimental conditions. There are three major network model development efforts, all of which have benefited from Professor Suuberg's work on coal macromolecular structure, crosslinking behavior, modeling of pyrolysis kinetics, tar vaporization behavior, and the effects of pyrolysis on intrinsic char reactivity.

ACKNOWLEDGEMENTS

In addition to the authors, the work at Advanced Fuel Research, Inc. (AFR) has involved several individuals who are named in references [15-17,28,30,33-35,38-40,44,45]. Professor Eric Suuberg of Brown University consulted on many aspects of the model development effort. Professor Philip Best of the University of Connecticut also made important contributions. The support of the FG-DVC model development work by the U.S. Department of Energy, National Science Foundation, and the Department of Agriculture is gratefully acknowledged.

REFERENCES

1 Suuberg, E.M., Peters, W.A., and Howard, J.B., *Ind. Eng. Chem. Process Des.*, Dev. 17, 37-46 (1978).
2 Suuberg, E.M., Peters, W.A., and Howard, J.B., *17th Symp. (Int.) on Combustion*, p. 117, The Comb. Inst., Pittsburgh, Pa (1979).
3 Unger, P.E., and Suuberg, E.M., Fuel, 63, 606 (1984).
4 Suuberg, E.M., Unger, P.E., and Lilly, W.D., Fuel, 64, 956 (1985)
5 Suuberg, E.M., Lee, D. and Larsen, J.W., Fuel, 64, 1668 (1985).
6 Suuberg, E.M., Unger, P.E., and Larsen, J.W., Energy Fuels, 1, 305 (1987).
7 Unger, P.E. and Suuberg, E.M., *18th Symp.(Int.) on Combustion*, p. 1203, The Comb. Inst., Pittsburgh, PA (1981).
8 Suuberg, E.M., *Chemistry of Coal Conversion*, R. Schlosberg (Ed.), Chapter 4, Plenum (1985).
9 Suuberg, E.M., Peters, W.A., and Howard, J.B., *Thermal Hydrocarbon Chemistry*, ACS Symposium Series, A.G. Oblad, H.G. Davis and R.T. Eddinger (Eds) 183, pp. 239-257, Washington, DC (1979).
10 Suuberg, E.M., "Properties of Tars Produced During Pyrolysis – Significance in Combustion systems," paper presented at Eastern States Section of Combustion Institute, Atlantic City (1982).
11 Suuberg, E.M. *ACS Div. Fuel Chem. Prepr.* 32(3), 51 (1987).
12 Oja, V. and Suuberg, E.M. *Anal. Chem.*, 69, 4619 (1997).
13 Suuberg, E.M. in *Fundamental Issues in Control of Carbon Reactivity*, J. Lahaye and P. Ehrburger, Eds., NATO ASI Series No. 192, p. 269 ff, Kluwer Academic Publishers, Boston, 1991.

14 Solomon, P.R., Serio, M.A., and Suuberg, E.M., "Coal Pyrolysis: Experiments, Kinetic Rates and Mechanisms," *Prog. Energy Combust. Sci.*, Vol 18, pp. 133-220 (1992).
15 Solomon, P. R., Hamblen, D. G., Carangelo, R. M., Serio, M. A., and Deshpande, G. V., *Energy & Fuels*, 2, 405 (1988).
16 Solomon, P. R., Hamblen, D. G., Yu, Z. -Z. and Serio, M. A., *Fuel*, 69, 754 (1990).
17 Solomon, P. R., Hamblen, D. G., Serio, M., A., Yu, Z. -Z. and Charpenay, S. C., *Fuel*, 72, 469 (1993).
18 Grant, D. M., Pugmire, R. J., Fletcher, T. H., and Kerstein, A. R., *Energy & Fuels*, 3, 175 (1989).
19 Niksa, S., *Energy & Fuels*, 5, 647-683 (1991).
20 Ko, G. H., Sanchez, D. M., Peters, W. A. and Howard, J. B., *Twenty-Second Symp. (Intl) on Comb.*, p. 115, The Combustion Institute, Pittsburgh, 1988.
21 Neavel, R. C., Smith, S. E., Hippo, E. J., and Miller, R. N., *Proc. of Intl. Conf. on Coal Sci.*, p.1, Dusseldorf, Sept. 1981.
22 Niksa, S., *Energy & Fuels*, 8, 659-679 (1994).
23 Niksa, S., *Combust. Flame*, 100:384 (1995).
24 Niksa, S., *Energy & Fuels*, 9, 467 (1995).
25 Zhao, Y., Serio, M.A., Bassilakis, R., and Solomon, P.R., *Twenty-Fifth Symposium (Int.) on Combustion*/The Combustion Institute, pp 553-560, (1994).
26 Fletcher, T.H., Kerstein, A.R., Pugmire, R.J., Solum, M.S., and Grant, D.M., *Energy & Fuels*, 6:4, p. 414-431 (1992).
27 Stauffer, D., and Aharony, A., *Introduction to Percolation Theory*, 2nd Edition, Taylor & Francis, London, UK, 1991.
28 Charpenay, S., Serio, M.A. and Solomon, P.R., "The Prediction of Coal Char Reactivity Under Combustion Conditions," *24th Symposium (Int) on Combustion*, The Combustion Institute, Pittsburgh, PA, 1189-1197 (1992).
29 Vorres, K. S., Energy & Fuels, 4(5), 420 (1990).
30 Wójtowicz, M.A., Serio, M.A., and Bassilakis, R., "Pyrolysis yields and kinetics for coal originating in different parts of the world," submitted to the *10th International Conference on Coal Science* , Taiyuan, China, (September 12-17, 1999).
31 Niksa, S., *ACS Div. of Fuel Chem. Preprints*, 43(1), 131 (1998).
32 Perry, S.T., and Fletcher, T.H., *ACS Div. Of Fuel Chem. Preprints*, 43 (1), 141 (1998).
33 Wójtowicz, M. A., Zhao, Y., Serio, M. A., Bassilakis, R., Solomon, P. R. and Nelson, P. F., in *Coal Science: Proceedings of the Eighth International Conference on Coal Science* (J.A. Pajares and J. M. D. Tascon, Eds.), Coal Science and Technology, vol. 24, Elsevier, Amsterdam, 1995, pp. 771-774.
34 Solomon, P.R., Serio, M.A., Hamblen, D.G., Smoot, L.D., Brewster, B.S., Radulovic, P.T., Final Report (Vol. 2) under DOE Contract No. DE-AC21-86MC23075 (October 1986 – September 1993).
35 Solomon, P.R., Serio, M.A., Zhao, Y., Wojtowicz, M.A., Smoot, L.D., Brewster, B.S., Radulovic, P.T., Topical Report under Contract No. DE-AC21-93MC30040.
36 FLUENT ACERC Module User's Guide, Version 1 (October 1996).
37 Jones, J.M., Patterson, P.M., Pourkashanian, M., Rowlands, L. and Williams, A., "An advanced coal model to predict NO_x formation and carbon burn-out in pulverised coal flames," presented at the 14th Annual International Pittsburgh Coal Conference & Workshop, Taiyuan, China, September 23-27, 1997.
38 Zhao, Y., Chen, Y., Hamblen, D.G., and Serio, M.A., *Proceedings of the 9th International Conference on Coal Science*, Essen, Germany (September 7-12, 1997), pp. 645-648.
39 Serio, M.A., Nelson, C.M., Chen, Y., Final Report for NSF Grant DMI-9761057 (October, 1998).
40 Zhao, Y., Serio, M.A. and Solomon, P.R., *26th Symposium (Int.) on Combustion*, The Combustion Institute, Pittsburgh, PA, 3145-3151 (1996).
41 Matthews, J.P., Hatcher, P.G., Scaroni, A.W., *ACS Div. of Fuel Chem. Preprints*, 43(1), 136 (1998).
42 Kumagai, H., Norinaga, K., Hayashi, J.-I., and Chiba, *Proceedings of the 1998 International Symposium on Advanced Energy Technology*, 2-4 February 1998, Sapporo, Japan, pp. 61-68.
43 Takanohashi, T., Iino, M., and Nakamura, K., *Proceedings of the 1998 International Symposium on Advanced Energy Technology*, 204 February 1998, Sapporo, Japan, pp. 77-84.
44 Serio, M.A., Solomon, P.R., Kroo, E., Bassilakis, R., Malhotra, R., and McMillen, D., *Proceedings of the 1991 Int. Conf. on Coal Science*, New Castle, England, Butterworth-Heinemann, Oxford, (1991).
45 Charpenay, S., Serio, M.A., Bassilakis, R., and Solomon, P.R., *Energy and Fuels*, 10(1),26 (1996).

NANOSTRUCTURES IN COAL-DERIVED CARBONS

Robert Hurt, Joseph Calo, Ying Hu
Division of Engineering
Brown University
Providence, RI 02912

INTRODUCTION

Carbon nanostructure, the local spatial arrangement and orientation of graphene layers, affects many important properties of carbon materials, including mechanical strength and modulus [1,2], coefficient of thermal expansion [2], electrical properties [3] and their directional dependencies, pore size distribution [4,5], and reactivity to oxidizing gases [5]. In coal-derived carbons in particular, the nanostructure influences surface area and fine porosity of coal-derived sorbents, coke strength and gas reactivity, and the graphitizibility of anthracites. This paper examines the fundamental mechanisms that determine nanostructure in carbon materials, with special emphasis on coal as the organic precursor. In common with Professor Suuberg's studies of tar vapor pressures, this work involves the physical chemistry of pyrolysis and carbonization.

RESULTS AND DISCUSSION

Figure 1 shows two example nanostructures in flame-derived coal chars. Structure A exhibits long range orientational order with statistical fluctuations (meandering) about the mean orientational vector. This nanostructure is believed to arise through liquid crystal formation during the fluid stage of carbonization. Structure B exhibits only short range orientational order, in the form of recognizable "crystallites". In some carbons these crystallites are oriented completely at random, while in the lignite char sample in Fig. 1B there is some degree of preferential orientation among the crystallites. The following sections discuss the quantitative description of these structures and the mechanisms of their formation.

Quantification of order

HRTEM fringe images allow quantification of nanostructure by digital image analysis [6-8]. The results are best described as semiquantitative, due to the extremely small sample size probed by the electron beam and the difficulty obtaining statistically significant data for correlation to bulk sample properties. The order parameter, $S = 1/2 < 3 \cos\theta - 1 >$ is a measure of long-range anisotropy, where θ is the angle between a single layer (or line in 2D) and the mean orientational vector, and $<>$ denotes an average. If the anisotropy extends over supramicron length scales it can be easily detected by optical microscopy (where it is referred to as coke texture) and quantified as the difference between the minimum and maximum reflectance upon optical stage rotation under polarized light (optical bireflectance).

Determination of the long-range order parameter for the structures in Fig. 1 yields 0.9 for structure A and 0.6 for the structure B. An analysis based on liquid crystal theory has shown that the 0.9 order parameter is consistent with a liquid crystal formation mechanism, while 0.6 is not [8]. The low grade orientational order in the lignite sample is believed to be caused by strain induced alignment during carbonization [8].

Phase behavior of PAH mixtures

The formation of anisotropic carbon via the liquid crystal route can be treated as a problem in liquid / liquid phase equilibrium [9,10]. As molecular weight increases during carbonization, so does aspect ratio of the oligomers formed from the primary aromatic clusters. At a critical aspect ratio, the oligomers undergo a concerted alignment to form the ordered fluid, which upon further molecular weight growth undergoes a glass transition to form a solid carbon. In PAH mixtures, phase separation occurs in which the higher molecular weight components partition preferentially into the liquid crystalline phase, and lower molecular weight components into the isotropic phase. Further polymerization causes the mesophase (LC phase) to grow at the expense of the isotropic phase until one or both phases solidify.

The quantitative description of this phase behavior is complicated by the lack of model compound studies showing this behavior. Indeed, no pure polyaromatic hydrocarbon has ever been observed to form a discotic liquid crystal! A recent analysis suggests that this paradox is a mixture effect [10]. In complex multicomponent PAH mixtures, crystalline solid phases are suppressed and the underlying liquid crystalline phases are revealed. Figure 2 illustrates this effect in a hypothetical binary mixture. In multicomponent calculations, it is possible for a mixture of N nonmesogens to give rise to liquid crystalline phases due to the severe depression of the liquid / solid phases transition temperatures.

The latent liquid crystal forming tendency in PAH increases with increasing molecular weight (for similar structures), and in a complex mixture, the entire molecular weight distribution influences whether or not the liquid crystalline phase appears. Macroscopic

solution thermodynamics can be used to estimate the amount and compositions of the isotropic and anisotropic phases given the overall molecular weight distribution of the melt [10]. This solution thermodynamics approach is not valid in the low molecular weight limit — i.e. it does not give the correct results for solvents with no liquid crystal forming tendency (nonmesogens). Statistical models based on pseudo-potentials for orientation give a useful description of nonmesogen behavior [9], but are difficult to solve in the general multicomponent case involving N mesogens with differing molecular weights and clearing temperatures. More work is needed to develop comprehensive, tractable equilibrium models of mesophase formation.

Role of Fluidity

In low viscosity pitches, mesophase typically appears as Brooks-Taylor mesospheres, which are thermodynamically favored as they possess the minimum mesophase / isotropic interfacial area. The high viscosities in coal carbonization prevent this thermodynamic state from being reached and lead to irregularly-shaped anisotropic domains. Nonfusible material can also limit the growth and coalescence of mesophase by collecting at the boundaries between the mesophase and isotropic phases or between mesophase regions (domains) of different orientation.

At still lower mobility (higher viscosity), the primary formation of carbonaceous mesophase is suppressed, and the resulting carbon has very short range orientational order (5 - 10 nm). Figure 3 shows results of a numerical simulation that addresses the effect of layer mobility on liquid crystal phase transitions [11]. The simulations employ hard lines which rotate and grow in a two-dimensional continuum. At high mobility (rotational frequency) the lines adopt orientational order at a certain length to avoid overlap. At lower mobility, the lines form finite ordered regions in an isotropic matrix, thus mimicking the observed behavior of carbons. Figure 4 plots the order parameter as a function of the dimensionless mobility-to-growth ratio. The numerical model in its simplest form is sufficient to distinguish two important classes of carbon materials: (1) isotropic carbons formed via all-solid-state routes in which molecular mobility is severely limited (e.g. low-rank coals, woody and cellulosic materials, and oxygen-rich thermosetting polymers), and (2) anisotropic carbons formed from precursors that pass through a mobile, liquid-phase intermediate (high-rank bituminous coals, polyvinyl chloride, anthracene, many petroleum and coal-tar pitches).

It is further found that anthracitic order can be adequately represented by simulations in which the layers have a preferred initial direction (non-zero initial order parameter) and non-zero initial length (see Fig. 4). This is justified by TEM and NMR studies of raw anthracites which indicate that significant aromatic cluster development has occurred during coalification. The simulations in Fig. 4 show a gradual, monotonic increase in final order as the mobility increases, so that anthracites produce chars with long-range order intermediate between the high-rank bituminous coals and the low-rank materials. This simulation behavior is consistent with the observed rank trends.

Figure 5a,b show further comparisons between carbonization studies and the simple numerical simulations. Figure 5a shows measurements of optical bireflectance as a function of carbonization temperature for three coals of various rank [12]. These results are given as a function of temperature, rather than time, but are indicative of the solid structures observed during the various stages of carbonization, as they might occur during non-isothermal heat treatment. The lowest rank coal is isotropic it its initially state and remains essentially so during carbonization. The high-rank bituminous coal shows measurable anisotropy it its raw state, but loses this anisotropy at 400 °C, and regains it at slightly higher temperatures. Apparently the increase in mobility on heating allows the structure to relax from a metastable configuration imposed by high lithostatic pressure to a near equilibrium isotropic configuration at 1 bar pressure. As heating continues, molecular weight growth proceeds until the planar structures reach the critical size (aspect ratio) for liquid crystal formation, and a highly ordered state develops. The bireflectance thus passes through a minimum, as seen in Fig. 7 in the curve labeled high-rank bituminous. The anthracite in raw form shows significant anisotropy, which is unaltered up to 600 °C and then slightly enhanced by higher temperature heat treatment. Despite the high degree of initial order, the anthracite does not develop the same degree of order as the high-rank bituminous coal. This is consistent with the observation that many anthracites are nongraphitizable [13].

Finally, Fig. 5b shows time dependent simulation results for three cases representing important classes of coals. The simulations show that: (1) the low rank coal is nearly isotropic and remain so during carbonization, (2) the high rank bituminous coal loses its initial anisotropy, but regains it during the latter stages of carbonization, (3) the anthracite retains and slightly enhances its anisotropy during carbonization. Comparing Figs. 5a and 5b, it is seen that the simple hard-line simulations also mimic these major trends seen in the bireflectance studies. Overall, the concepts of liquid / liquid equilibrium, together with the kinetic effects associated with limited layer mobility can describe the formation of most carbon types. An exception, however, is isotropic coke, whose formation mechanism receives separate consideration in the next section.

Isotropic coke

Many coal chars pass through a fluid state, but solidify to form isotropic chars. The lack of long range order in these materials cannot be explained by low fluidity (high viscosity) — many of them exhibit higher maximum fluidities than coals which form anisotropic chars. A promising explanation for isotropic coke formation is the suppression of liquid crystalline phases by non-planar molecules, or "non-mesogens".

A key requirement for the formation of liquid crystalline phases is a high aspect ratio, L/D, of the rod-like or disk-like constituent molecules. Most functional groups that act as cross-linking agents for aromatic clusters (aryl, ether, sulfide) involve non-linear single bonds. These cross-links produce oligomers of aromatic clusters that can adopt both planar and nonplanar configurations upon bond rotation. Depending on the shape of the aromatic oligomer (influenced by the geometry of the aromatic clusters and side chains) the planar geometries may be stearically hindered, and the nonplanar structure that results may act as a "nonmesogen" and cause a local disruption in the liquid crystalline phase.

The effect of nonmesogens on LC phases has been studied in the canonical case of spherical solutes (L/D = 1) in rod-like mesogens [14]. Phase diagrams for binary mixtures of mesogens and nonmesogens have been derived from a statistical theory based on a pseudo-potential for orientation. Recently, Shishido [9] have applied this statistical theory to explain the suppression of mesophase in pitch by addition of low-molecular weight pitch fractions (which were presumed to be completely nonmesogenic).

Figure 6 presents a qualitative picture of this effect as it may occur during coal carbonization. Assuming a linear relationship between clearing temperature and molecular weight [10], the Bates-Shishido phase diagram can be plotted as MW vs. the mole fraction nonmesogen. The plot also shows two possible carbonization trajectories for a high-rank and low-rank bituminous coal. The trajectories were calculated using the measured elemental composition of the solid carbonizing phase, and assuming that a fixed fraction, F, of the oxygen and sulfur atoms were present as in functional groups that lead to non-planar cross-links. The average number of these non-planar groups per oligomer is:

$$N = F\,(X_{O+S})\,(MW_{oligomer}) / (MW_{mixture})$$

where X_{O+S} is the mole fraction O and S atoms, and $MW_{mixture}$ is the mean atomic weight of the carbonizing melt. The mole fraction nonmesogens is then the probability that a given oligomer contains one or more non-planar links (and thus has an overall nonplanar geometry), which, assuming a Poisson distribution, is given by: 1 - exp(-N).

Trajectories were drawn for various values of F in an attempt to reproduce the experimental fact that Illinois #6 flame chars are isotropic, while Pocahontas #3 chars are anisotropic (except for inertinite-derived material). A value of 0.05 gives reasonable behavior as shown in Fig. 6. Thus if only 5% of the O and S atoms are involved in nonplanar cross-linking structures, liquid crystal formation will be largely suppressed in the low-rank Illinois #6 coal. This is the most promising explanation for the overall trend of isotropic coke formation from many oxygen-rich and sulfur-rich precursors. The full quantitative relation between chemical functionality and mesogenicity is, of course, complex and must be based on functional group analysis rather than simple elemental analysis.

It is evident from this paper that much more work is needed before we have a complete quantitative understanding of the origin and evolution of carbon nanostructures.

REFERENCES

1. Emmerich, F.G. *Carbon* 33 47 (1995).
2. Sato S., Kawamata, K., Kurumuda, A., Kawamota, M., Ishida, R. *Carbon* 26 (4) 465 (1988).
3. Rouzaud, J.N., Oberlin, A. *Carbon* 27 (4) 517 (1989).
4. Oberlin, A., in *Chemistry and Physics of Carbon, Vol. 22*, ed. P. A. Thrower, Marcel Dekker, New York, 1989, pp. 1-143.
5. Rouzaud, J.N., Oberlin, A. Chapt. 17 in *Advanced Methodologies in Coal Characterization*, Elsevier, Amsterdam, 1990.
6. Palotas, A. B., Rainey, L. C., Feldermann, C. J., Sarofim, A. F., and Vander Sande, J. B., *Microsc. Res. Tech.*, 1996, 33, pp. 266-278.
7. Dobb, M. G., Guo, H., and Jonhson, D. J., *Carbon*, 33 1115 (1995).
8. Shim, H.S., Hurt, R.H., Yang, N.Y.C. "A Methodology for Analysis of 002 LF Fringe Images and Its Application to Combustion-Derived Carbons", *Carbon*, in press.
9. Shishido, M., Inomata, H., Arai, K, Saito, S. *Carbon* 35 (6) 797 (1997).
10. Hurt, R.H., Hu, Y. "Thermodynamics of Carbonaceous Mesophase," *Carbon*, in press, 1998.
11. Hu, Y., Calo, J.M., Hurt, R.H., Kerstein, A. "Kinetics of Orientational Order / Disorder Transitions and Their Application to Carbon Material Synthesis," *Modelling and Simultion in Materials Science and Engineering*, in press.
12. Murchison, D.G., Chap. 31 in *Analytical Methods for Coal and Coal Products*, Academic Press, New York, 1978.
13. Blanche, C., Dumas, D., Rouzaud, J.N. Coal Science (Pajares and Tascon Eds.) Elsevier Science, Amsterdam, 1995, p. 43.
14. Humphries, R.L., and Luckhurst, G.R. *Proc. R. Soc. London, A.* 352 41-56 (1976).

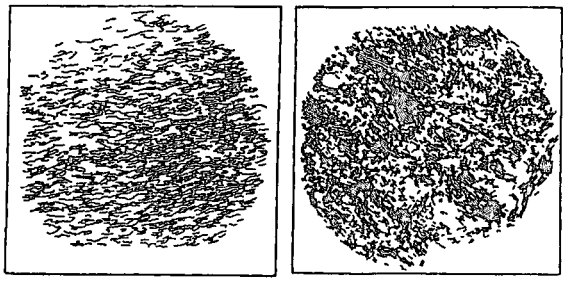

A B

Figure 1. Digitally enhanced high resolution TEM fringe images showing the nanostructures of coal-derived carbons. The lines are graphene layers, imperfect snippets of the graphite lattice, viewed edge-on. A: Pocahontas #3 char; B: lignite char.

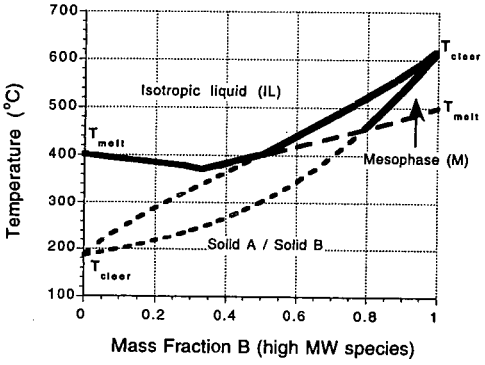

Figure 2. Example binary phase diagram for generic PAH of low and high molecular weight. In the pure state A is nonmesogenic and B is mesogenic.

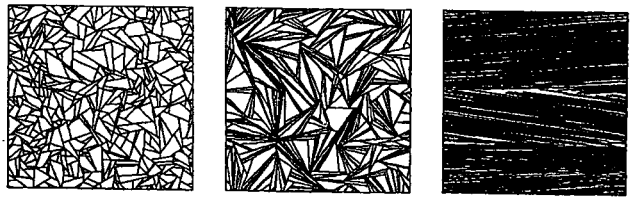

M* = 0 M* = 37 M* = 2,200

Figure 3. Summary of frozen states in hard-line simulations. As mobility/growth ratio, M*, increases, the final structures changes from complete disorder to short range order to a structure in which the ordered length scale is comparable to the size of the simulation box.

Figure 4 Summary of final states in numerical simulations starting from initially random states (isotropic parent materials) and initial ordered states (anisotropic parent materials). Long-range order parameter in the final state vs. dimensionless mobility / growth ratio, M^*. Curve labels show the relation to carbonization processes. Type A carbons: isotropic solids formed through solid-state pyrolysis (e.g from lignites, woody tissue, oxygen-rich polymers); Type B carbons: anisotropic solids formed through liquid phase pyrolysis (pitches, polyaromatic compounds, coking coals); Type C carbons: anisotropic solids formed by solid-state pyrolysis of initially *ordered precursors* (e.g. anthracites).

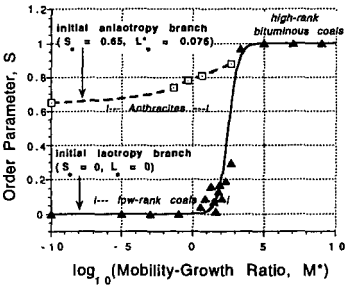

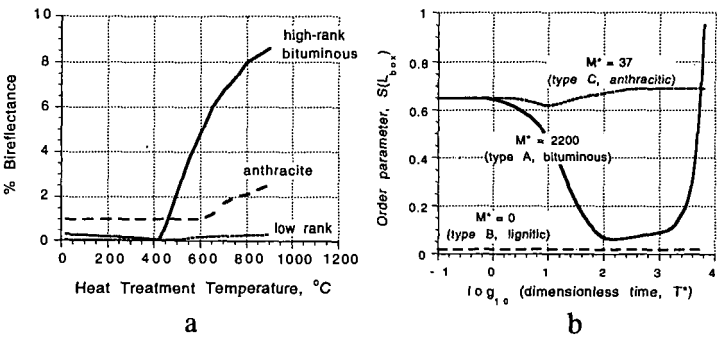

Figure 5. a: Measurements of optical birefectance as a function of carbonization temperature for three important classes of coals from Murchison [12]; b: Time evolution of the long-range nematic order parameter in three simulations representing important classes of carbonization processes.

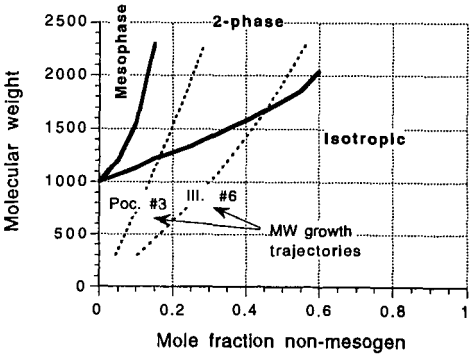

Figure 6 Phase diagram for binary mixture of mesogens and nonmesogens showing possible trajectories describing the carbonization of bituminous coals of different rank. Plot is useful for developing a theory of isotropic coke formation.

THE GASIFICATION REACTIVITY OF CARBONS - NEW DEVELOPMENTS

Eric M. Suuberg
Division of Engineering, Brown University, Providence, RI 02912

Keywords: Coal, carbon, surface area, porosity, gasification, combustion

Introduction

The reactions of chars (or "carbons") with oxidizing gases are among the most important of industrial reactions. Basic to utilization of any solid fuel, and important in processes ranging from activated carbon production to steel-making, they have been extensively studied for more than a century, e.g., 1,2. It is a tribute to the complexity of the processes involved that they have not yet yielded to intensive study, and a quantitatively predictive description of the phenomenon is not yet in hand. The difficulties in developing such a quantitative description are well-known. First, the materials from which the carbons are derived leave an indelible imprint on their character. Second, the temperature history of their preparation also has a significant impact. Modeling the complexity of the relevant pyrolysis processes still represents an imposing challenge (see the presentation by Serio et al. in this symposium). Third, the presence of small amounts of additional elements, serving as catalytic agents, influence both the course of carbon formation and subsequent gasification behavior. Finally, subtle aspects of combined phase and reaction behavior can drive the morphology of the carbons across a wide spectrum of characteristics (see the presentations by Hurt et al. and Winans et al. in this symposium). These morphological differences also play a key role in the subsequent reaction behavior of the carbons, as it is the ability of the oxidizing gases to gain access to the porosity in the carbon which determines some key aspects of the reaction process. Improvements in the quantitative description of these phenomena will require experimental examination of all of these processes at a greater level of detail. No single study will be able to provide all of the pieces, and progress will continue to be achieved through many fundamental examinations of various aspects of the processes. In this presentation, a key focal point will be the question of how porosity develops during gasification processes, and what this tells us about several of the above issues.

Patterns of Porosity Development

One useful new tool in the examination of this question is the use of NO as a model reactant. The reaction rates of carbons with NO are generally intermediate between the rates of carbon with oxygen on the one hand and those with CO_2 or steam on the other hand. Relatively few systematic studies of NO-carbon reactions have been undertaken; activation of carbons in NO is not of known commercial interest and the role of the carbon-NO reaction is of debated significance in practical combustion systems (they appear to clearly be of importance in fluidized beds, but probably of lesser importance in pulverized systems, except perhaps during reburning). Various aspects of the reaction have been recently reviewed[3].

Figure 1 shows that for gasification of a Wyodak coal-derived char in the intrinsic reaction rate regime, the development of *microporosity* follows a qualitatively similar pattern in three oxidizing gases (O_2, CO_2, NO), but there exist quantitative differences between the pattern in CO_2 and in the other gases. Experimental details have been provided elsewhere[4]. Characterization of porosity is here based upon traditional N_2 isotherm-derived quantities, but other adsorptives support the

Figure 1. Wyodak coal char surface area evolution in different oxidizing gases.

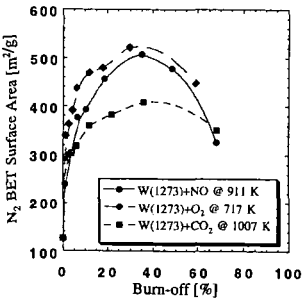

Figure 2. Wyodak coal char mesopore volume evolution in different oxidizing gases

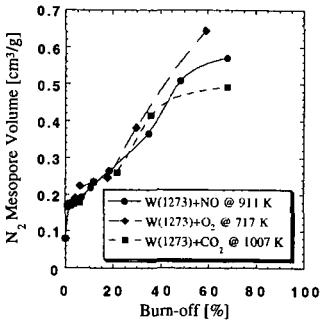

conclusions[4]. The development of *mesoporosity* also follows a very similar pattern in all three gases, even quantitatively up to a certain point, see Figure 2. These results emphasize that some

care is required in selection of data, and criteria, for drawing conclusions regarding the universality (or lack thereof) in a pattern of porosity development.

The so-called random pore models of gasification[5,6] have adopted the viewpoint that there is a single structural parameter which can be used to describe the relationship between conversion (extent of gasification) and porosity in the char. Figure 1 would require viewing this parameter as a a function of both starting material and gaseous environment. Figure 2, however, speaks to the possibility of viewing the structural parameter as a true material constant, at some level of approximation. Existence of a material-specific structural parameter is supported by results such as shown in Figure 3, illustrating development of porosity in a microcrystalline graphite, and Figure 4 showing development of porosity in a char derived from pine wood. Here, the data on porosity are shown as adsorption isotherms. Again, gasification conditions were selected so as to give comparable (apparently intrinsic) rates in all gases.

Figure 3. N_2 isotherms for graphite gasified in three gases (open points- desorption).

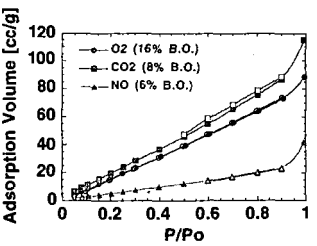

Figure 4. N_2 isotherms for pine char reacted in three gases (adsorption isotherms).

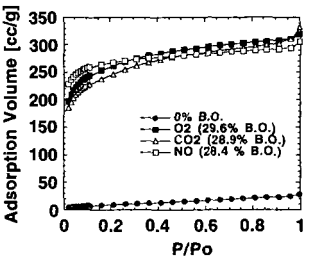

These two cases represent extremes of behavior observed in many other materials. The graphite sample starts with virtually no porosity (the isotherm is at the bottom of the figure) and develops only fairly large-scale porosity (meso- and macroporosity), consistent with pitting of the surface. This is seen in Figure 3 as an increase in slope of the isotherms in the mid- to high- range of P/Po, and this slope increases with burn-off. On the other hand, the char derived from pine shows a dramatic upward shift with burn-off of the isotherms in the low P/Po range, indicating opening of microporosity. There are only modest change in meso- and macroporosity. The isotherms for the Wyodak material described in Figures 1 and 2 can be viewed as a composite of these two behaviors, consistent with the development of both types of pores.

It is clear from the above that the nature of activation is, to a first approximation, a property of the material and not of the reactant gas. The great importance of starting material is well known to those concerned with activated carbons. The reasons for these differences in porosity development patterns are not, however, entirely understood in all cases. It is fairly certain that the graphite cannot develop microporosity because of the locus and nature of the attack on its surface - the oxidizing gases are known to attack edge atoms, dislocations, etc., and this can only happen where the gases have access to such sites on the external surface. The pine char has a highly disordered structure to begin with, and a great deal of porosity, providing reactant gases access to its interior. Some of the dramatic increase in micropore volume in Figure 4 is an artifact of the well-known problem of activated diffusion of nitrogen at the low temperatures of measurement of the isotherms, but a large part is not, and there appears to be true development of both microporosity (and some mesoporosity). Does this require penetration of the reactant gases on the micropore size scale, as has been often suggested? It is unclear at the present time.

There can be no doubt that catalysis can play an important role in influencing the course of the observed processes. Figures 5 and 6 illustrate the mesopore size distributions observed after gasification of the Wyodak char in its original and demineralized states. The pore size distributions were calculated using the Barrett-Joyner-Halenda (BJH) method, corrected for micropore volumes[7]. This type of calculation is often criticized on various theoretical grounds, but the qualitative conclusions are very clear. The original Wyodak char, which is known to contain an abundance of catalytic mineral matter, develops very similar mesoporosity in all three gases (consistent with Figure 2). After demineralization, there is little mesoporosity development over the same range of burn-off. It is believed that it is the catalyst particles which in some manner dictate the development of the mesoporosity in the original sample, a conclusion consistent with the limited literature on this topic[8].

The above results notwithstanding, the results of Figure 1 show, as does much of the literature on activation of carbons, that the development of porosity during reaction of carbons in different gases can show distinct patterns, even if the reaction rates are closely matched, e.g., ref. 8. The results of Figures 3 through 6 appear to directly contradict a conclusion that CO_2 and O_2 will necessarily

Figure 5. Pore size distributions for Wyodak char gasified in three gases.

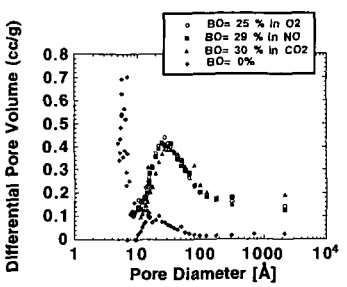

Figure 6. Pore size distributions for demineralized Wyodak char gasified in NO and CO_2.

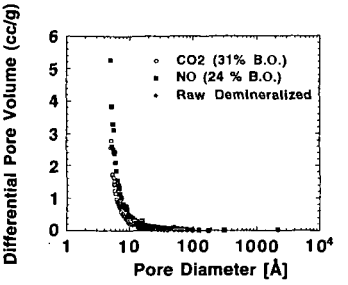

involve a very different pattern[8], but it is important to note that sometimes differences emerge only at higher burn-offs. Again, the reasons for the initial similarity and subsequent divergence are not yet understood. What does appear to be clear is that the differences are not an artifact of the choice of adsorptive used for examining porosity - both nitrogen and CO_2 isotherms offer similar conclusions. The other conclusion which may be drawn is that the simple, empirical porosity development models cannot yet handle this issue.

Annealing

In the gasification and combustion literature, there is a well-established pattern of decrease in reactivity with increase in heat treatment temperature[9-19]. This phenomenon has often been termed annealing, on the basis that heat treatment "heals" the surface, removing the imperfections that constitute the main active sites. We have empirically modeled the process as involving an extension of high-temperature pyrolysis phenomena. The activation energy distributions characteristic of pyrolytic release of hydrogen merge with the activation energy distributions characteristic of graphitization. The distributed activation energy approach has been quite successful in predicting the changes in reactivity with heat treatment[12,20].

What has remained unclear is what physical factors are most important in determining the change in reactivity with heat treatment. Is the phenomenon tied to the gradual perfecting of aromatic structure, associated with the growth of condensed aromatic structures? Success has been achieved in correlating reactivity with hydrogen remaining in the structure[21]. Or is the loss of active sites mainly attributable to a loss of surface area with heat treatment? Both factors are sure to contribute to differing extents in different situations. In some cases, loss of catalyst or catalyst dispersion has also been cited.

The simple picture of reactivity loss with heat treatment is further complicated by several recent findings. First, there is the observation that annealing does not proceed at the same rate with respect to NO reactivity as it does with respect to oxygen reactivity[3]. In the case of NO, the annealing of a phenolic char could be entirely explained on the basis of surface area changes, whereas in the case of oxygen, there was an effect beyond surface area change involved. Another issue which has received attention recently is "memory loss" in gasification. As gasification conversion increases, differences in reactivity attributable to differences in heat treatment tend to disappear[11,22]. The effect has been attributed to selective burn-off of less ordered material early in the process, leaving behind increasingly similar more ordered and less reactive residues as conversion increases. What occurs is, however, not so clear when data on active site concentration variations with burn-off are considered. Figure 7 shows these trends in a phenolic resin char, in which active surface area (ASA) was determined by oxygen chemisorption[23]. As burn-off increased, the more highly heat treated char approached the less highly heat treated char in both total surface area (TSA) and ASA. Meanwhile, the 573 K oxygen gasification reactivities of the samples slowly approached one another, in the usual fashion. What this means is that by one measure of structure and reactivity, the highly heat treated sample is becoming more reactive with burn-off. By the other measure, the less heat treated sample is declining in reactivity, while the more highly heat treated is remaining more or less the same. Clearly these results call into question the assay of ASA by oxygen chemisorption, and its significance with respect to high temperature gasification rates. But these results also suggest that the penetration of porosity by the oxygen reactant may be quite different in different reaction regimes; in the low temperature chemisorption regime, the oxygen reaches different porosity than in the higher temperature regime. This is, in fact, the basis of an exciting new carbon activation process being developed by AFR, Inc.[24].

Figure 8 shows that the more highly heat treated char develops a larger porosity than does the less heat treated char (again relying on a BJH-type pore size distribution analysis). The N_2 surface areas of these two samples are within about 15% of each other. Thus it seems possible that the

Figure 7. Reactivity and ASA variation in phenolic resin chars heat treated for 2 hours at indicated temperatures.

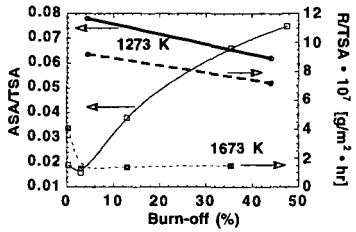

Figure 8. Pore size distributions for chars of Fig. 7, after approx. 20% burn-off in oxygen.

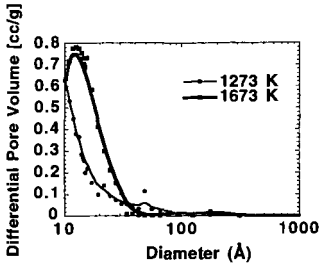

very different ASA behaviors are a consequence of the creation of more large porosity, in the case of the 1673 K char, and may not really be a good indicator of truly available ASA at high temperatures.

Surface Area and Reactivity

It has been recognized for quite some time that the rate of gasification of a carbon should in some way be related to its surface area. The above data and discussion have perhaps already raised concerns regarding how difficult it might be to assess the correct surface areas. Historically, two main methods have been employed for measuring the areas. One involves the use of nitrogen isotherms and the BET equation, and the other involves use of carbon dioxide isotherms and some form of the Dubinin-Radushkevich equation. The relative merits of both methods have been debated for some time. While it is true that activated diffusion barriers are sometimes a problem for N_2 adsorption at liquid nitrogen temperatures, the importance of this issue has perhaps been overplayed. Carbon dioxide is, on the other hand, often unable to interrogate the larger micropores[7]. It has thus been recommended that a combination of both probes be used to avoid drawing false conclusions[7]. We have recently examined a number of adsorptives on the same chars, and concluded that there was no particular advantage to use of carbon dioxide over nitrogen[4].

Reactivity data for the Wyodak chars are shown in Figure 9, again using the three main oxidizing gases of this study. All of these data show an increase in reactivity per mass of remaining carbon, with burn-off (note that the behavior in this case was only tracked to 70% burn-off). The question of whether the reactivities could be normalized by surface areas was then examined. Figure 10 shows the results of normalization by BET surface areas. The only special feature of this normalization is that the reactivity at 1% burn-off was taken as the reference, in order to avoid

Figure 9. Reactivity of Wyodak char in different oxidizing gases.

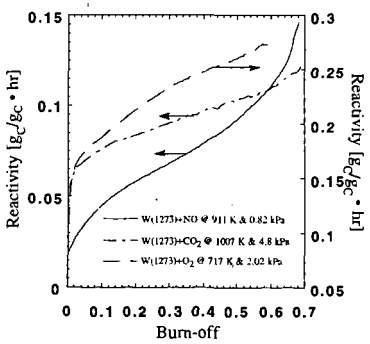

Figure 10. Normalized reactivities of Wyodak char.

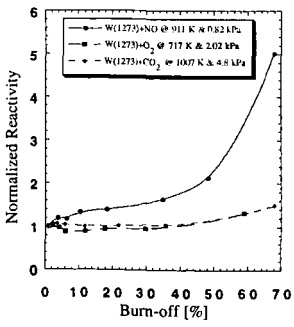

issues related to severe activated diffusion limitations leading to apparently low BET areas at near zero burn-off. Thus if surface area truly normalizes reactivity, a horizontal line should be obtained at unity. Such is very nearly the case in oxygen and in carbon dioxide, but not in NO. Still, caution must be exercise in concluding that reactive gases can reach all of the available micropore surface areas in the cases of oxygen and carbon dioxide. It was suggested in connection with Fig. 5 that the main locus of reaction may be catalyst particles. In such a case, an apparent correlation of reactivity with surface area may be indirect; catalyst area may correlate with micropore area for some reason. In any case, a correlation with surface area might actually only be a correlation with numbers of micropores, and reactants may be unable to use any more than the mouths of the micropores. Suggestions that micropores might not be fully utilized in reaction are numerous[5,16,25,26].

The case of NO reactivity was particularly interesting. In the case of this reactant, the normalization appeared to be poor. Examined more closely, the curve for NO does, however, show a period of relatively constant reactivity per unit of surface area. This has been taken to indicate that the normalization reactivity per unit area (at 1% burn-off) was actually too low, in this case by about 50%, since the period of constant reactivity occurs at a normalized value of about 1.5 . This in turn indicates that the microporosity initially present was not all available for reaction, and was only opened up by 10% burn-off. Beyond 40% burn-off, the curve begins to rise sharply once again. This is further indication that the original normalization was based upon the wrong (too high) surface area. Only as the microporosity is opened up (becomes wider) does NO gain greater access to the surface. This was verified by sharp changes in the pore size distributions in this range of burn-offs. Thus, the use of BET or DR surface areas to normalize reactivities is of little fundamental significance, and should be approached with great caution.

Summary

Results have been obtained for a wide range of carbons, which suggest that the development of porosity is most strongly dependent upon the nature of the starting material. Gasification environment can play a role in porosity development, as may the presence of catalysts. Annealing of the carbon influences its porosity and therefore, accessibility of reactant gases. Surface areas for reaction of gases with carbons are a useful concept, but the methods presently used to normalize reactivities must be viewed as essentially empirical. There is evidence to suggest that micropore surfaces are not available for reaction.

Acknowledgment

The important contributions of former graduate students are most gratefully acknowledged, in particular, those of Indrek Aarna, Marek Wójtowicz and Hsisheng Teng. The financial support of the NSF, under grant BES- 9523794, is also gratefully acknowledged.

References

1. Walker, P.L., Jr.; Rusinko, F., Jr.; Austin, L.G. *Adv. Cat.* **1959**, *XI*, 133.
2. Essenhigh, R.H. in *Chemistry of Coal Utilization, Second Supplementary Volume*, M. Elliott, Ed., Chap. 19, Wiley, 1981.
3. Aarna, I.; Suuberg, E.M. *Fuel*, **1997**, *76*, 475.
4. Aarna, I.; Suuberg, E.M. *27th Symp. (Int.) on Comb.*, in press, 1998.
5. Gavalas, G.R. *AIChEJ*, **1980**, *26*, 577.
6. Bhatia, S.K.; Perlmutter, D.D. *AIChEJ*, **1980**, *26*, 379.
7. Rodríguez-Reinoso, F.; Linares-Solano, A., in *Chemistry and Physics of Carbon, Vol. 21*, P. A. Thrower, Ed., p. 1, Dekker, New York, 1989.
8. Rodriguez-Reinoso, F.in *Fundamental Issues in Control of Carbon Gasification Reactivity*, J. Lahaye, P. Ehrburger, Eds. p. 533 , Kluwer Academic, Dordrecht, 1991.
9. van Heek, K.H.; Mühlen, H.J. *Fuel*, **1985**, *64*, 1405.
10. Duval, X. *Ann. de Chem., 12th Ser.*, **1955**, *10*, 58.
11. Senneca, O.; Russo, P.; Salatino, P.; Masi, S. *Carbon*, **1997**, *35*, 141.
12. Suuberg, E.M. in *Fundamental Issues in Control of Carbon Gasification Reactivity*, J. Lahaye, P. Ehrburger, Eds. p. 269, Kluwer Academic, Dordrecht, 1991.
13. Serio, M. A.; Solomon, P.R.; Bassilakis, R.; Suuberg, E.M. *ACS Div. Fuel Chem. Prepr.* **1989**, *34(1)*, 9.
14. Beeley, T.; Crelling, J.; Gibbins, J.; Hurt, R.; Lunden, M.; Man, C.; Williamson, J.; Yang, N. *26th Symp (Int.) on Comb.* p. 3103, The Combustion Institute, Pittsburgh, 1996.
15. Jenkins, R.G.; Nandi, S.P.; Walker, P.L., Jr. *Fuel*, **1973**, *52*, 288.
16. Radovic, L.R.; Walker, P.L., Jr.; Jenknis, R.G. *Fuel*, **1982**, *62*, 849.
17. Gale, T.K.; Bartholomew, C.H.; Fletcher, T.H. *Energy Fuels*, **1996**, *10*, 766.
18. Kasaoka, S.; Sakata, Y.; Shimada, M. *Fuel*, **1987**, *66*, 697.
19. Sahu, R.; Levendis, Y.; Flagan, R.; Gavalas, G. *Fuel*, **1988**, *67*, 275.
20. Hurt, R.H.; Sun, J.K.; Lunden, M. *Comb. Flame*, **1998**, *113*, 181.
21. Charpenay, S.; Serio, M.A.; Solomon, P.R. *24th Symp (Int.) on Comb.* p. 1189, The Combustion Institute, Pittsburgh, 1992.
22. Anxustegi, M.M.; Calo, J.M.; Hurt, R.H.; Shim, H. S. *Proc. Eurocarbon '98*, p. 675, GFEC, 1998.
23. Suuberg, E.M.; Wójtowicz, M.; Calo, J.M. *Carbon*, **1989**, 27, 431.
24. Wójtowicz, M.; Markowitz, B.L.; Simons, G.; Serio, M.A. *ACS Div. Fuel Chem. Prepr.* **1998**, *43*, 585.
25. Hurt, R.H.; Sarofim, A.F.; Longwell, J. *Fuel*, **1991**, *70*, 1079.
26. Dutta, S.; Wen, C.Y.; Belt, R.J. *Ind. Eng. Chem. Proc. Des. Dev.* **1977**, *16*, 20.